Open Journal of Neuroscience

ROSS Science Publishers

Research Article

OPEN ACCESS

Viral and Non-viral Tracing of Cerebellar Corticonuclear and Vestibulorubral Projections in the Mouse

Lynn W. Sun[*]

James H. Clark Center for Biomedical Engineering and Sciences, 318 Campus Drive West, Room W080, Stanford University, Stanford, California, 94305, USA

Corresponding Author & Address:

Lynn W. Sun[*]

James H. Clark Center for Biomedical Engineering and Sciences, 318 Campus Drive West, Room W080, Stanford University, Stanford, California, 94305, USA; Tel: (650) 799-5848; Email: lynnsun@alumni.stanford.edu

Published: 30th April, 2013 Accepted: 30th April, 2013

Received: 7th March, 2013

Open Journal of Neuroscience, 2013, **3**-3

ABSTRACT

Previously reported multisynaptic tracing of the mouse eyeblink circuit [1] revealed characteristic spatiotemporal patterns in cerebellar labelling that suggested well-defined corticonuclear pathways. This project further explores the connectivity of these circuits in the cerebellum and in downstream motor structures. Cerebellar cortical projections to the deep cerebellar nuclei were traced with retrograde virus, which was allowed to propagate through one infection cycle (synapse). Further downstream motor circuits were traced with electroporated dextran dye and fluorescent microbeads. Distinct, coherent pathways were uncovered from ansiform lobule to the dentate nucleus, from the lobule simplex to the anterior interpositus, from anterior vermis to posterior interpositus, and from posterior vermis to fastigial nucleus. There were no cross-projections observed between the corticonuclear projections to different cerebellar nuclei. The first two pathways have been implicated in classical conditioning, while the third is likely involved in cerebellar modulation of reflexes, as well as in the control and enhancement of conditioned responses. Little is known about the fourth, and its potential motor outputs were further explored by tracing from the fastigiovestibular tract to the red nucleus and vice versa, establishing the existence of a previously unexplored vestibulorubral pathway in the mouse.

INTRODUCTION

Cerebellar corticonuclear projection pathways remain relatively undefined in the mouse. In previous experiments [1], transsynaptic Pseudorabies virus (PRV-152) infusions in the mouse eyelid revealed characteristic spatiotemporal labelling patterns in the cerebellum. PRV-expressed Green Fluorescent Protein (GFP) labelling propagated to the fastigial nuclei initially and reached the interpositus and dentate nuclei after a delay of several hours. A similar medial-to-lateral pattern emerged in the deep cerebellar nuclei (DCN), with vermal regions of the cerebellar cortex exhibiting labelling first, followed by paravermal regions, and finally by hemispheric regions. These patterns may result from well-organized, spatially distinct corticonuclear pathways wherein lateral regions of the cerebellar cortex project to the lateral deep cerebellar nuclei while medial regions of the cortex project to the medial nuclei. Importantly, corticonuclear pathways may be relatively localized with no overlap between corticonuclear pathways. That is, a given portion of the cerebellar cortex found to project to a certain cerebellar nucleus will not send axon collaterals to a different nucleus.

This project attempts to trace and identify

these potential corticonuclear pathways in the cerebellum. Previously, corticonuclear tracings have been attempted in rat and cat using older tracing methods, and the results of these experiments [2-12] largely agree with the corticonuclear circuit hypotheses previously mentioned. However, such experiments have never been performed with modern unidirectional tracers, and these putative projections have never been mapped in the mouse. Finally, although the downstream motor outputs of the anterior, posterior and dentate nuclei have been explored, and although the fastigiovestibular projection is well established [13], vestibulorubral projections have only been explored in non-mouse experiments [14].

This project attempts to systematically address previous gaps in knowledge by employing modern transsynaptic (PRV-152), monosynaptic (Red RetroBead) and dye-electroporation methods. PRV offers robust, self-sustaining labelling [15-19]; Red RetroBeads allows simple, dependable single-step tracing, and electroporated dyes provide very fine targeting of small structures [20]. Using these tools, the pattern and connectivity of cerebellar corticonuclear projections and fastigial projections to downstream motor nuclei were investigated. Generally, findings supported a developing view of distinct, orderly, non-overlapping corticonuclear pathways which may form an anatomical framework supporting the multiple motor functions of the cerebellum.

MATERIALS AND METHODOLOGY

Viral Culture

Viral experiments used the EGFP-expressing Pseudorabies virus, PRV-152. A detailed overview of the PRV-152 virus can be found in [21]. Virus was grown in PK-15 cells using an adapted version of Card and Enquist's protocol [17]. Immediately prior to usage, viral suspension was sonicated to rupture any intact cells. The aliquot was further centrifuged at 2000 x g for 5 minutes at room temperature to remove cellular debris. Viral batches were regrown every 6 months to maintain potency, and titers ranged between $8.9x10^8$ to $1.2x10^9$ IFU/mL.

Surgery

All experiments presented in this article conformed to guidelines laid down by the NIH in the US regarding the ethical care and use of animals for experimental procedures. Experiments approved by the Institutional Animal Care and Use Committee (IACUC) at Stanford University, also known as the Administrative Panel on Laboratory Animal Care (APLAC), and were designed to minimize the number of animals used and their suffering. 9 week old male C57Bl/6 mice were used throughout studies. Animals were anesthesized using a ketamine/xylazine cocktail administered intraperitoneally and mounted on a Kopf Model 900 stereotaxic frame. For pressure injections of PRV-152 and Red Retrobeads (LumaFluor), a World Precision Instruments UltraMicroPump (UMP3) and SYS-Micro4 Controller unit was mounted onto the stereotaxic frame in order to deliver microinjections via a 33-gauge needle mounted on a Hamilton precision syringe. For electroporation of dextran-conjugated dyes, a Multichannel Systems STG 1004 stimulus generator was used to generate all electroporation currents, and a standard Kopf electrode holder was used to mount the electrode and glass capillary onto the stereotaxic frame in preparation for surgery.

In all intracranial infusions, a 1cm incision was made along the midline of the scalp using a scalpel. The skull was leveled and a dental drill was used to bore a small hole in the skull over the injection location. The needle/electrode was then lowered down to the injection site. After 5 minutes, injection/electroporation was initiated. Pressure injections were made at a rate of 50nL per minute. 100 nL of EGFP-expressing PRV-152 were injected in each retrograde corticonuclear tracing experiment, while 250 nL of red RetroBeads were injected in each retrograde vestibulorubral tracing experiment. More red RetroBeads were injected due to the relatively large size of the target nucleus and the relatively low uptake and transfer of red RetroBeads versus self-propagating virus. In electroporation experiments, anionic, lysine-fixable fluorescein-conjugated 3000MW dextran (Molecular Probes Invitrogen) was prepared at a 10% w/v solution. A ground electrode was clipped to the base of the tail and a -50uA square-wave 50ms current was pulsed at 2Hz for 20 minutes. After injection/electroporation was complete, the needle/electrode was left in place for another 5

minutes and then slowly withdrawn. The wound was closed with VetBond (3M) and/or skull staples (Fine Science Tools). Animals were returned to cages and monitored until conscious, then returned to holding cages for an incubation period of 2 days.

Intracranial injections of virus were highly effective, and virtually all animals were infected after inoculation. Similarly, virtually all electroporations and dye injections resulted in potent labelling. However, due to the very small size of target nuclei, not all injections were successfully localized. Thus, all animals were histologically examined post-mortem to determine furthest extent of viral/Retrobead spread, based on visible fluorescence in situ. Animals in which injections were determined to be misplaced and/or too large were excluded from data collection, and maps were ultimatedly generated from injections that were histologically confirmed to be successful. Only successfully injected animals are included in final N-counts, which are as follows: N = 9 for PRV injections into the fastigial nucleus; N = 14 for PRV injections into the interpositus nuclei (10 anterior, 4 posterior); N = 11 for PRV injections into the dentate nucleus. N = 12 for Red RetroBead red nucleus pressure injection experiments. N = 7 for electroporation into the vestibular nuclei.

Histology

After sacrifice, excised brains were fixed overnight in ice-cold 4% PFA, washed for a minimum of 8 hours in PBS, and embedded in newly prepared 4% agarose gel. A Leica VT1000S vibratome was used to take sequential 100 µm coronal slices. Each brain was sliced from the posterior margin of the cerebellum to the anterior margin of the cerebellum. For experiments using PRV, additional antibody staining was required. Slices were blocked in 1% w/v bovine serum albumin (BSA, Sigma-Aldrich) and 3% goat serum (Sigma-Aldrich) in PBS for 1 hour at room temperature. They were then incubated in 1% w/v BSA/1% goat serum/1:500 rabbit anti-GFP antibody (Molecular Probes Invitrogen) in PBS for 48 hours at 4oC. Secondary antibody solution was prepared similarly using a 1:1000 dilution of AlexaFluor 488-conjugated goat anti-rabbit antibody (Molecular Probes Invitrogen) and incubated for 60 minutes at room temperature.

Imaging and Mapping

Slices were mounted using Fluoromount G (Southern Biotech) under #0 or #1 coverslips sealed and examined for labelled cells using a Leica M216 FA variable-magnification fluorescent stereo microscope. Epifluorescent images were taken using a Q-Imaging Retiga 4000RV camera. Confocal images were taken using a Leica SP2 AOBS confocal laser scanning microscope. All maps were produced using Neurolucida 7 (MBF Biosciences). A standardized map was first created by tracing nuclei of note in the unstained, fixed brain of a 9 week old male C57Bl/6 mouse sliced at 100 µm intervals. Every specimen slice found to contain labelled neurons was then matched to the closest approximate section in the standardized template. Neurons were mapped throughout the thickness of the slices, and every eGFP-expressing neuron observed was mapped using Neurolucida. This process was repeated for every animal to create a consolidated, interactive Neurolucida map of all available tracing data. For ease of publication, this map was then broken down by experiment.

RESULTS AND OBSERVATIONS

Single-step retrograde tracing from the deep cerebellar nuclei (DCN) reveals discrete, nonoverlapping corticonuclear projections.

Representative raw images of injections and virally labelled cells in the cerebellum are presented in Figure 1. Although PRV is a transsynaptic virus, the short incubation times of experiments presented in this manuscript generally only allowed time for a single infection cycle (a one-synapse propagation). PRV injection into the fastigial nucleus resulted in labelling in the posterior vermis. Labelled cells were distributed across the 9th and 10th lobules and along the vermis of lobules 6-8 (Figure 1A). PRV injection into the anterior interpositus nucleus resulted in labelling in the simple lobule and the lateral 6th cerebellar lobule (Figure 1B). AIP injections resulted in very focal, dense labelling along the mediolateral axis, as did PIP injections. However, PIP injections labelled Purkinje neurons in the anterior cerebellar lobules. Finally, PRV injection into the dentate nucleus resulted in mediolateral labelling in the hemispheric ansiform lobule (Crus 1 and Crus 2).

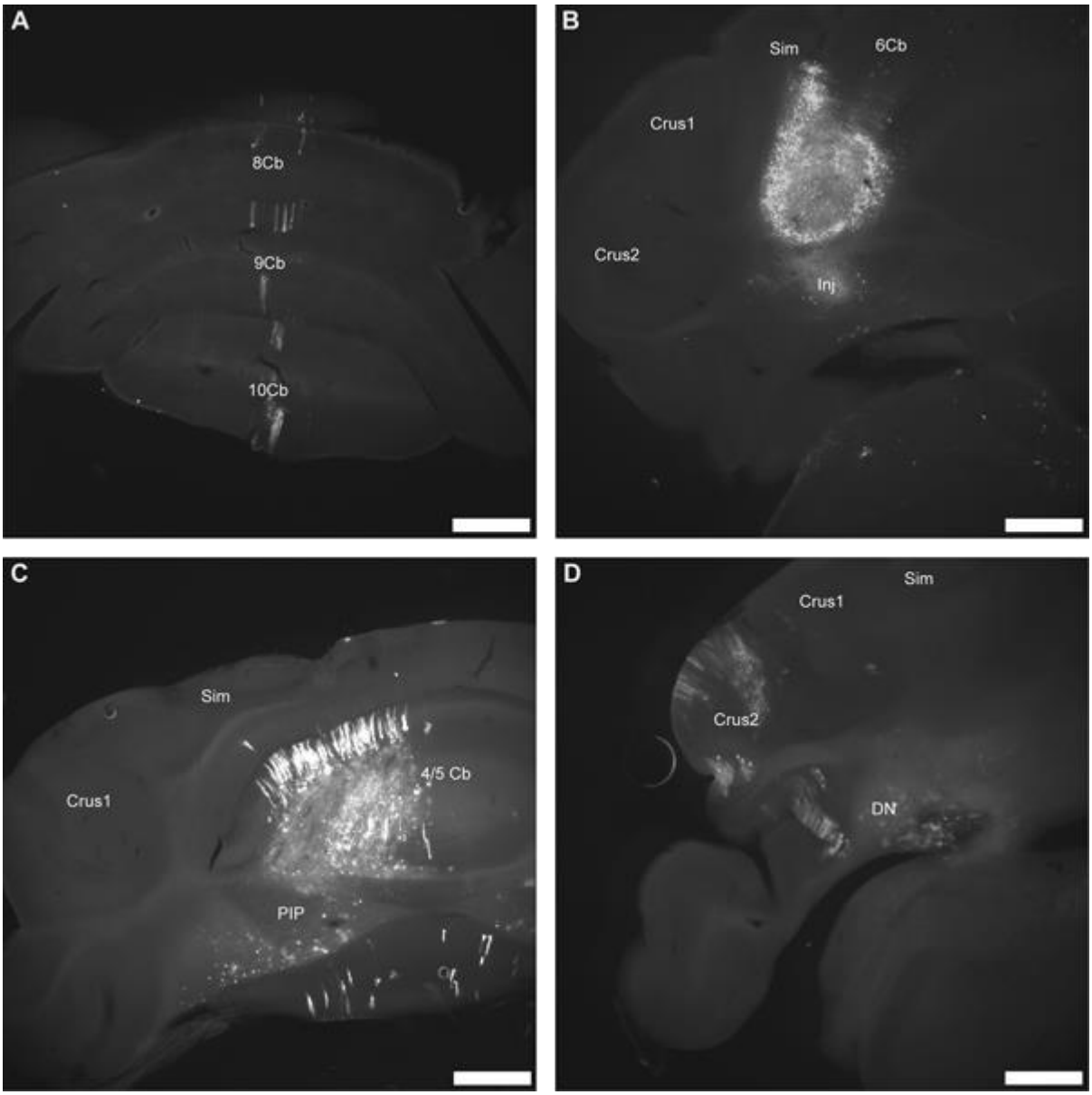

Figure 1: PRV injection into the deep cerebellar nuclei label distinct portions of the cerebellar cortex.

A. PRV injection into the fastigial nucleus results in labelling in the posterior vermis. Scalebar: 500 µm. **B.** PRV injection into the anterior interpositus nucleus results in labelling in the simple lobule and the lateral 6th cerebellar lobule. Axon tracts can be seen leaving the injection site (Inj). Scalebar: 500 µm. **C.** PRV injection into the posterior interpositus nucleus results in labelling in the anterior cerebellar lobules. Axon tracts can be seen leaving the injection site (Inj). This animal also showed sparse labelling in the 10th cerebellar lobule. Scalebar: 500 µm. **D.** PRV injection into the dentate nucleus results in hemispheric ansiform lobule (Crus 1, Crus 2) labelling. When a smaller, sub-saturating amount of virus is injected, some banding becomes apparent. The injection site is visible in this slice as a region of labelled neurons in the dentate nucleus (DN). Scalebar: 1 mm.

In all cases, injection sites appeared as areas of diffuse fluorescence. Incoming axon projections are often visibly labelled, as in Figure 1B and 1C. Transsynaptically labelled cells fluoresced brightly. In areas of high staining, labelled neurons often appeared as a consolidated band of fluorescent cells (Figure 1B, 1C). At lower viral titers, viral labelling was distinctly banded (Figure 1D). Injection into the DN, AIP and PIP resulted in heavy, mediolaterally-aligned labelling. In contrast, labelling from FN injections was sparser, and banded rostrocaudally across several lobules.

Compiled maps of all injections and staining are displayed in Figures 2, 3, and 4. The following patterns of projection emerged: ansiform lobule to dentate, simple lobule to anterior interpositus,

anterior paravermal lobules to posterior interpositus, and posterior vermal lobules to fastigial nucleus. Transsynaptic labelling arising from injections into each DCN appears in a distinct portion of the cerebellum with no apparent cross-projection. For example, dentate nucleus injections were never seen to label vermal Purkinje cells, and fastigial nucleus injections were never seen to label ansiform lobule Purkinje cells. The follow sections will examine patterns of labelling in greater detail.

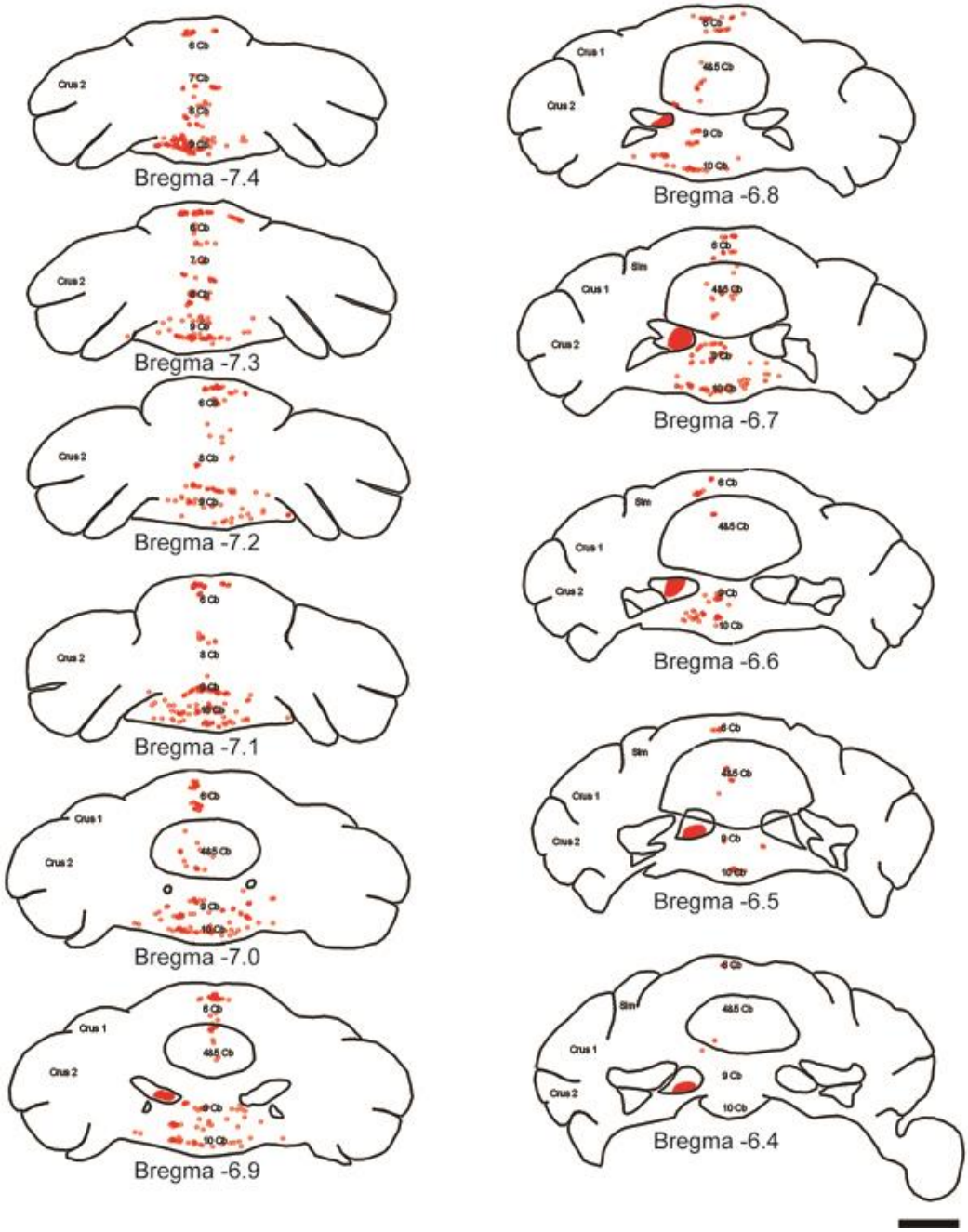

Figure 2: Composite maps of posterior and vermal labelling from fastigial nucleus injections.

2 days after PRV injection into the fastigial nucleus, scattered labelling appears in the cerebellar cortex along the vermal/paravermal axis of posterior cerebellar lobules 5 to 10. Scattered groups of labelled cells can be seen along the vermal axis, often crossing several lobules. Diagram shows composite maps of all animals with anterior interpositus injections. Contrast the rostral-caudal "stripes" of labelling that span several lobules with the focal, medial-lateral bands found in interpositus and dentate injections. Tracer injection sites are marked in red. Coordinates are expressed in millimeters caudal to bregma. Each point represents a labelled cell. Scalebar: 1mm.

Vermal and paravermal Purkinje cells project to the fastigial nucleus.

Injections into the fastigial nucleus labelled Purkinje cells in the vermal and paravermal areas of the cerebellar cortex (N = 9; Figure 1A, Figure 2). Labelling was relatively scattered and widespread across the medial cerebellar cortex, spanning from the 5th to the 10th lobules of the vermis (Figure 1A). The total volume over which labelled cells were found covered approximately 2mm in the medial-lateral direction, 1mm in the rostral-caudal, and 2-3mm in the dorsal-ventral direction (Figure 2). However, labelling was sparse within this area.

Labelled cells were more numerous in the posterior (8th, 9th and 10th) lobules, where they could be found throughout the lobule in the medial-lateral direction. In other lobules, labelled neurons were generally concentrated along the vermal axis. Furthermore, labelling originating from fastigial nuclear injections was unique in that eGFP-expressing neurons appeared along rostral-caudal columns, whereas injections into other deep cerebellar nuclei yielded medial-lateral rows of labelled cells. Labelled neurons typically did not appear in heavy mediolateral bands, but instead appeared banded across a narrow portion of the vermis. PRV-labelled neurons often appeared to align across interlobular folds, as can be seen in Figure 1A and 2, suggesting that alignment occurred in the rostrocaudal direction instead of the mediolateral direction.

Lateral 6th lobule and simple lobule Purkinje cells project to the anterior interpositus.

Injections into the anterior interpositus nucleus resulted in concentrated, localized staining on the lateral rim of the 6th cerebellar lobule and the medial side of the simple lobule (N = 10; Figure 1B, Figure 3A). This labelling contrasted labelling originating from the fastigial nucleus in several ways. Compared to fastigial-projecting neurons, anterior interpositus-projecting Purkinje cells were densely distributed within and sharply confined to a smaller portion of the cortex. Neurons labelled from the same injection spanned medial-laterally, and Purkinje cells projecting to the interpositus nucleus were found across a significantly smaller total volume of approximately 800um in the medial-lateral direction, 400um in the rostral-caudal direction, and 2mm in the dorsal-ventral direction (Figure 3A).

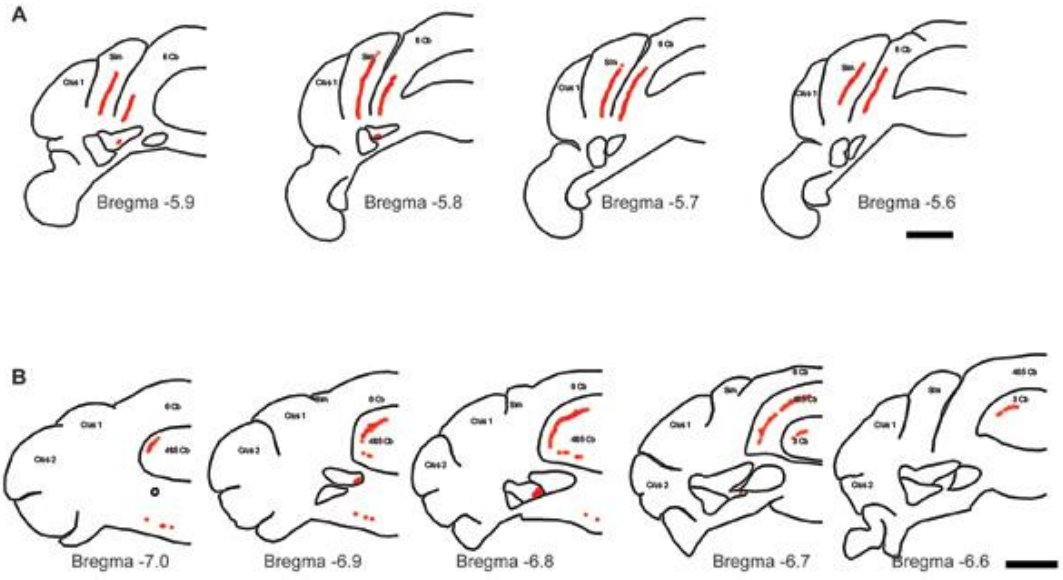

Figure 3: Composite maps of simple lobule labelling from anterior interpositus injections and paravermal labelling from posterior interpositus injections.

A. 2 days after PRV injection into the anterior interpositus nucleus, focal, dense labelling appears in the Simple lobule and the hemispheric 6th lobule of the cerebellar cortex. Diagram shows composite maps of all animals with anterior interpositus injections. Tracer injection sites are marked in red. Coordinates are expressed in millimeters caudal to bregma. Each point represents a

labelled cell. Please note that labelled neurons located at the bottom of the Lobule VI-Lobule Simplex fold have been standardized to either side of the fold on the map. Scalebar: 1 mm. **B.** Labelling appears in the paravermis of the 3rd, 4th and 5th cerebellar lobules 2 days after injection into the posterior interpositus nucleus. Diagram shows composite maps of all animals with posterior interpositus injections with tracer injection sites marked in red. Coordinates are once again expressed in millimeters caudal to bregma. Scalebar: 1 mm.

At high viral titers, labelled Purkinje cells formed a nearly uniform band of labelling in medial fold of the Simple lobule. At lower viral titers, or toward the rostral or caudal ends of the labelled section of the cerebellar cortex, more banding was apparent.

Purkinje Cells of the 3rd, 4th and 5th lobules project to the posterior interpositus.

PRV injections into the posterior interpositus resulted in concentrated and localized labelling similar to that found in anterior interpositus injections (N = 4; Figure 1C, Figure 3B). Labelling appeared primarily in the anterior cerebellar lobules 3, 4 and 5. A total area of 1.5mm medial-lateral, 500um rostral-caudal, and 2mm dorsal-ventral was covered (Figure 3B). Trace labelling was also found in the 10th cerebellar lobule in one case. However, due to the close proximity of the PIP and the fastigial nucleus (FN), which receives innervations from the 10th cerebellar lobule (Figures 1A, 2), it is possible that this labelling arose from viral diffusion into the FN.

As with AIP injections, heavy, near-uniform areas of labelling appeared when high viral titers were used. At lower viral titers or toward the edges of the labelled area, a banded pattern is more apparent in labelled Purkinje cells.

Ansiform lobule Purkinje cells project to the dentate nucleus.

PRV injections into the dentate nucleus, similar to injections into the interpositus nucleus, resulted in dense, localized staining spanning medial-laterally across Crus 1 and Crus 2 (ansiform lobule) of the hemispheric cerebellar cortex (N = 11; Figure 1D, Figure 4). Labelling was somewhat more diffuse than that observed in interpositus injections, however, and also spanned a somewhat greater total volume: approximately 1.5mm medial-laterally, 900um rostral-caudally, and 2-3mm dorsal-ventrally (Figure 4). Unlike labelling arising from anterior and posterior interpositus injections, labelled dentate-projecting Purkinje cells in the ansiform lobule generally exhibited banding regardless of viral titer or location.

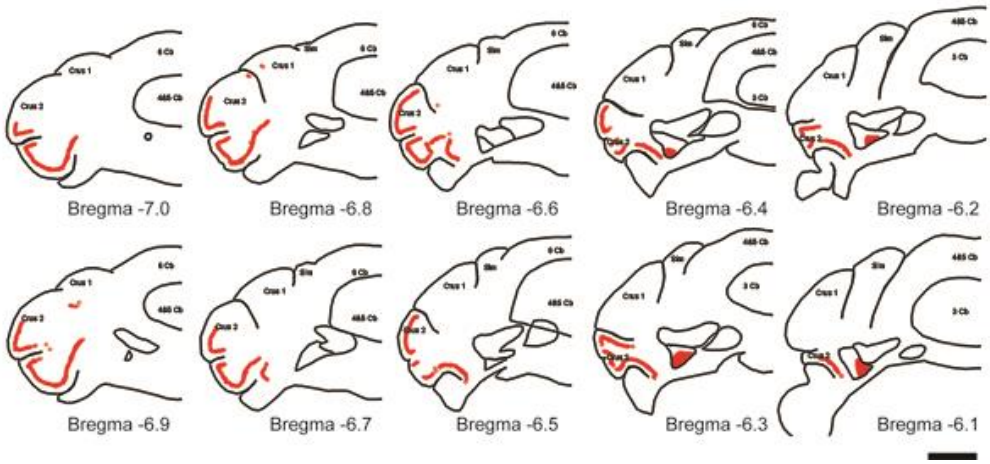

Figure 4: Composite maps of ansiform lobule labelling from dentate nucleus injections.

Labelled neurons in Crus 1 and 2 of the cortex appear in tight clusters. In areas of lighter labelling, some banding is apparent. Diagram shows composite maps of all animals with dentate injections. Tracer injection sites are marked in red. Coordinates are expressed in millimeters caudal to bregma. Each point represents a labelled cell. Please note that labelled neurons located at the bottom of the Crus 1-Crus 2 fold have been standardized to either side of the fold on the map. Scalebar: 1 mm.

Single-step retrograde tracing reveals a novel vestibulorubral tract in the mouse.

Downstream motor pathways of the interpositus and dentate nuclei are well-established, and the fastigiovestibular pathway has been conclusively identified in multiple model animals including the mouse. However, a vestibulorubral projection, which could serve as a motor output pathway for the vermal-fastigial circuit of the cerebellum, has not been previously characterized in the mouse. Using true (non-viral) single-step tracers in order to eliminate the possibility of false positive labelling via an unrelated multisynaptic pathway, vestibulorubral tracings were thus performed both in the anterograde and retrograde direction.

In the retrograde direction, fluorescent Red RetroBeads were injected into the area of the ventrolateral magnocellular red nucleus (Figure 5A) previously identified by eyelid injections of PRV. Close, well-defined clusters of labelled cells were found in both the anterior interpositus nucleus and the contralateral superior vestibular nucleus in each successfully injected animal (N = 12; Figure 5B). This provided evidence for a previously unreported vestibulorubral pathway in mice, which was confirmed in a followup experiment. Labelling in the vestibular nuclei was generally less robust than labelling in the AIP. Composite maps of data from all animals labelled via retrograde injection from the magnocellular red nucleus can be found in Figure 6.

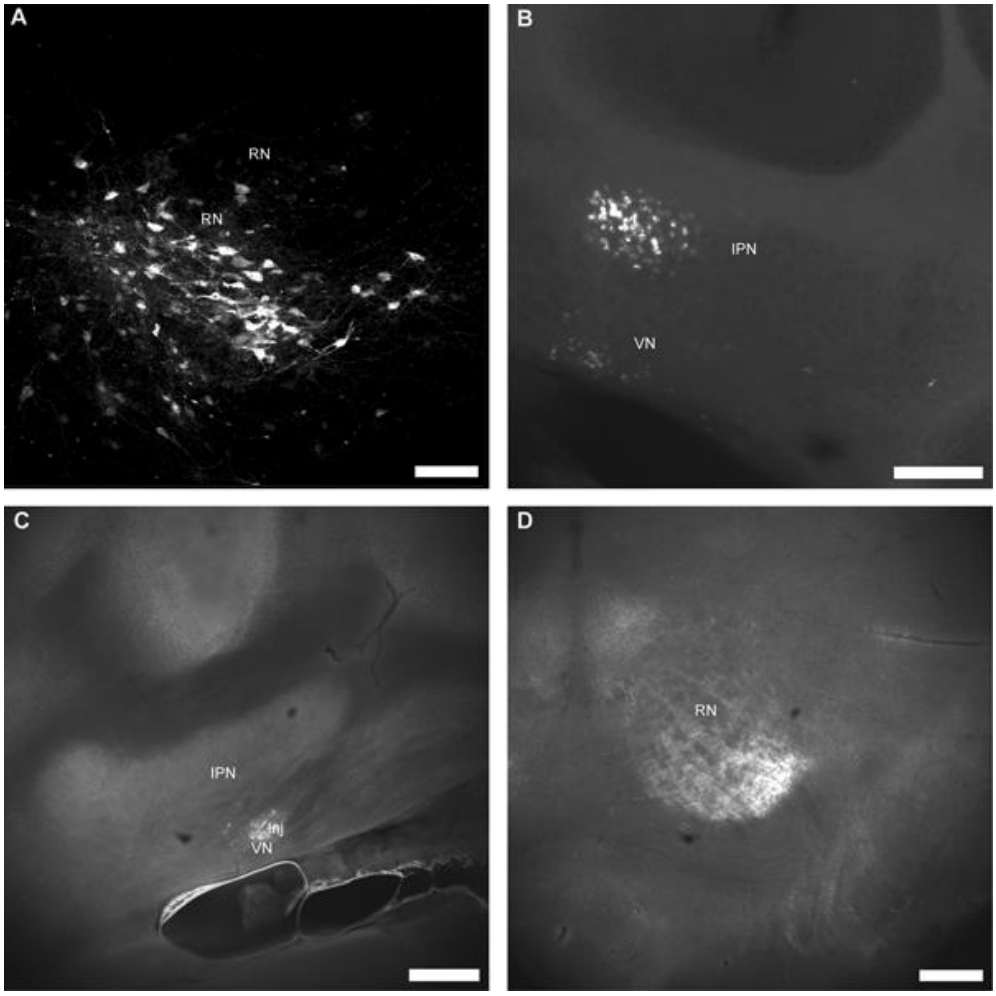

Figure 5: Single-step bidirectional tracing reveals a vestibulorubral tract in mouse.

A. Red RetroBeads injected into the red nucleus brightly labels neurons at the injection site. A high concentration of RetroBeads at the injection site results in very high-contrast labelling that persists for several days after infusion. Individual cells as well as diffuse fluorescence from diffused RetroBeads are visible. Scalebar: 100 µm. **B.** 2 days after Red RetroBead injection into the red nucleus, retrograde labelling appears in the contralateral IPN and VN. The contralateral superior vestibular nucleus shows clusters of labelled neurons in this image. Labelling was generally dimmer than concurrent labelling found in the anterior interpositus nucleus. Scalebar: 250 µm. **C.** Low-current electroporation delivers fluorescein-conjugated dextran focally to the superior vestibular nucleus. Image shows a representative injection site (Inj) in relation to nearly structures, including the anterior interpositus nucleus (IPN).

Scalebar: 250 mm. **D.** Fluorescein-conjugated dextran labels axon terminals from the vestibular nuclei to the contralateral red nucleus. Image shows brightly labelled axons terminating in the ventrolateral red nucleus. Scalebar: 250 µm.

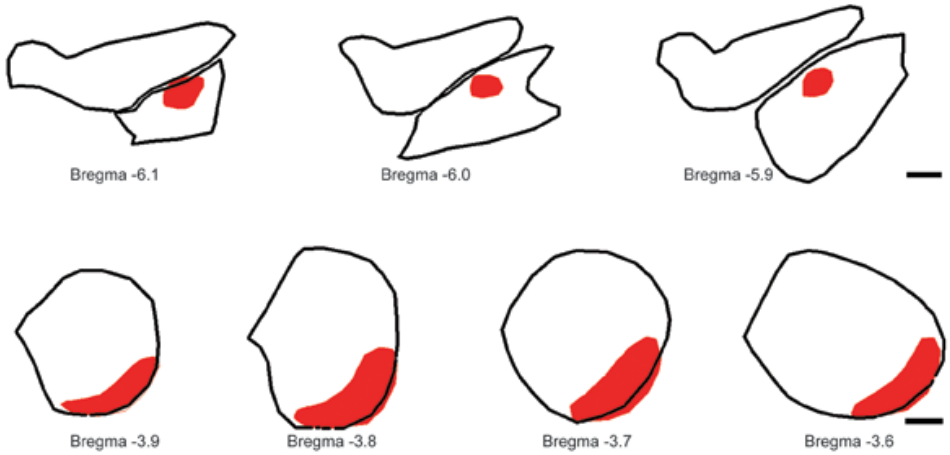

Figure 6. Composite maps of retrograde vestibular nuclei labelling after Red RetroBead injection into the red nucleus.

Top row: maximum extent of Red RetroBead retrograde labelling in the contralateral superior vestibular nucleus after injection into the red nucleus. Bottom row: maximum extent of Red RetroBead diffusion in red nucleus injection sites. Scalebars: 250 µm (top), 200 µm (bottom).

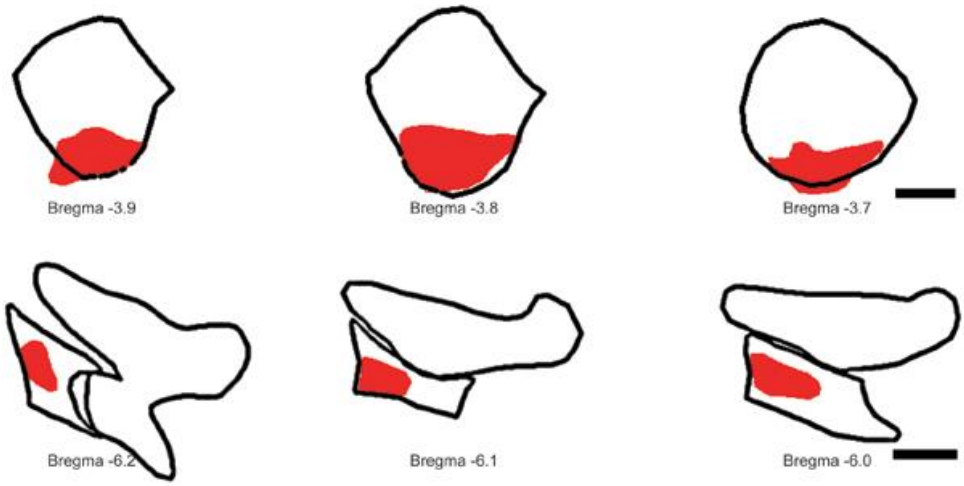

Figure 7: Composite maps of anterograde labelling in the contralateral red nucleus after fluorescently-conjugated dextran is electroporated into the superior vestibular nucleus.

Top row: maximum extent of axonal termination zones in the contralateral red nucleus after electroporation into the superior vestibular nucleus. Bottom row: maximum extent of electroporated areas in the superior vestibular nucleus. Scalebars: 200 µm (top), 250 µm (bottom).

Single-step anterograde tracing confirms a vestibulorubral tract in the mouse.

To confirm the vestibulorubral projection uncovered in the previous experiment, fluorescein-conjugated dextran was electroporated into the superior vestibular nucleus. Electroporation allows very fine, focal delivery of dye, which was critical in this experiment due to the extremely small size of the targeted portion of the superior vestibular nucleus. Furthermore, electroporation reliably fills the entirety of a labelled neuron without crossing the synaptic gap, allowing axon projections to be tracked from the point of electroporation to their downstream termination point.

A successful electroporation can be seen in Figure (5C). Axon tracts were followed from the

superior vestibular nucleus through the midbrain to their terminations in the contralateral ventral magnocellular red nucleus (N = 7; Figure 5D). Together, these two experiments offer evidence of an anatomic pathway through which vermal-fastigial input from the cerebellum may, via previously established pathways [22], modulate downstream motor behaviors.

DISCUSSION

Summary of Results

Figure 8 summarizes all circuitry explored in this body of work. Lower-order motor projections that were already well-established in previous literature [23-34] have been included for completeness. The experiments presented in this article consisted of single-step tracings addressing higher-order connectivity in the mouse. Corticonuclear projections were dissected with single-step retrograde tracings from each of the deep cerebellar nuclei, and a vestibulorubral tract was confirmed with both anterograde and retrograde single-step tracers.

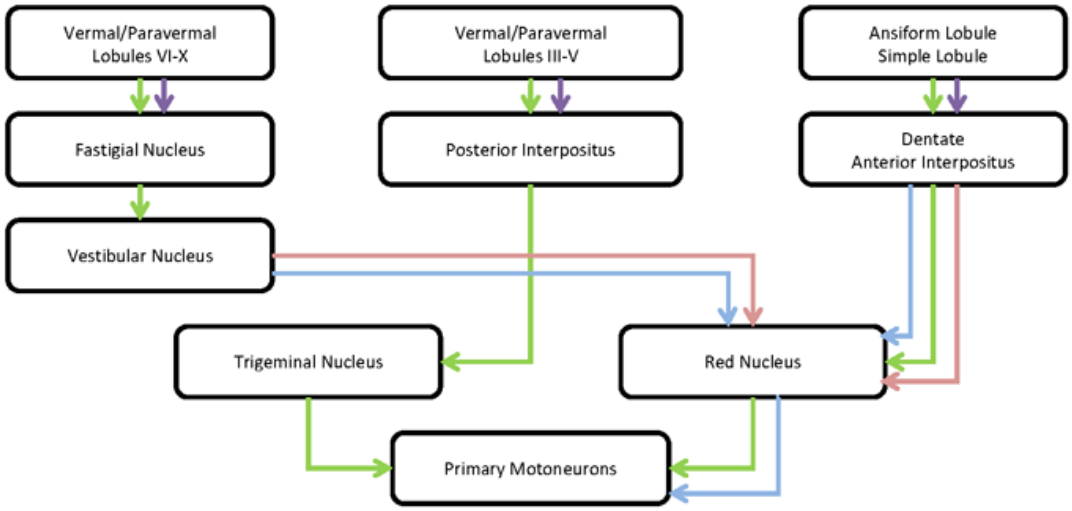

Figure 8: Summary Circuit Diagram

Green lines indicate pathways previously established in literature and in prior experiments. Red lines indicate single-step retrograde tracing with Red RetroBeads. Purple lines indicate single-step retrograde tracing with PRV-152. Blue lines indicate single-step anterograde tracing with electroporated fluorescein-conjugated dextran.

Results showed that Purkinje cells in the ansiform lobule (Crus 1 and Crus 2) of the CbCtx project to the dentate nucleus (DN). The hemispheric simple lobule (HVI) and the lateral portions of lobule 6 project to the anterior interpositus (AIP). The vermal and paravermal portions of anterior cerebellar lobules III-V project to the posterior interpositus (PIP), and the vermal portions of cerebellar lobules VI-VII, along with the vermal and paravermal portions of lobules VIII-X, project to the fastigial nucleus (FN).

Comparison to Previous Studies

A number of previous experiments have examined cerebellar corticonuclear projections in rat and cat models using older tracing methods. Dietrichs et al published a series of classic papers investigating corticonuclear neural circuitry using bidirectional transport of horseradish peroxidase (HRP) in the cat in the late 1970s and early 1980s [3-7]. These studies were followed by the Buisseret-Delmas et al studies in rat, which refined the bidirectional HRP technique by conjugation to a lectin, thus resulting in retrograde-only labelling [2, 35]. In recent years, Sugihara et al used a biotinylated dextran amine (BDA) to perform a series of elegant anterograde corticonuclear tracings in rat that yielded some of the most finely defined maps of cerebellar corticonuclear circuits to date [11, 12, 36].

These previous tracings found that the fastigial nuclei received input from the cerebellar vermis, the posterior interpositus nuclei from the paravermis, the anterior interpositus nuclei from medial areas of the hemispheres, and the dentate nuclei from lateral areas of the hemispheres [2, 3,

5-7, 11, 12, 36]. Furthermore, cortical areas corresponding to the FN were generally more discontinuous and broadly scattered than those projecting to the AIP, PIP, and DN [11, 36]. The studies presented in this manuscript broadly agree with these prior results.

However, Sugihara et al report that both anterior and posterior paravermal areas of the cerebellar cortex project to the posterior interpositus [11, 36], while experiments presented in this manuscript indicated only anterior paravermal corticonuclear projections to the PIP. Although this may be attributed to a difference between species, it is more likely that the small, localized injection area in this body of work, which was limited to the ventrocaudal PIP, only labelled a portion of all PIP-projecting Purkinje cells. Indeed, Sugihara further reports that anterior paravermal areas of the cerebellar cortex specifically project to the ventral PIP.

Putative Functions of Cerebellar Motor Circuits

Corticonuclear projections were uncovered with a series of single-step tracers. Results of these experiments provide strong evidence toward distinct, well-organized corticonuclear circuits. The pathways identified in the cerebellum, summarized in Figure 8, exhibited virtually no cross-projection. In other words, each pathway projected from and to spatially distinct regions of the cerebellum with no apparent overlap. Based on observations and experiments recorded in previous cerebellar literature, putative functions may be associated with each of the above hypothesized circuits.

The first of the circuits – from HVI to the AIP – is traditionally associated with classical conditioning. Work performed over the past 40 years has led to a general consensus that the interpositus nucleus, particularly the AIP, is critical to conditioning [9, 37, 38]. In the cerebellar cortex, HVI's contribution to conditioning has been thoroughly explored [39-44], but there is mounting evidence that the anterior lobules, in particular HIV and HV, may also contribute to, or even be crucial to, cerebellar conditioning [45-49]. Results from these experiments indicated that the hemispheric cortex projects to the AIP, while the anterior cerebellar cortex project to the PIP.

The second circuit projects from lobules III, IV and V to the PIP. The posterior interpositus previously been implicated in cerebellar reflex modulation, particularly in relation to the reflexive blink – a behavioral response to sudden or expected noxious stimuli to the eye and periorbital areas [24, 25]. Previous work done by the Evinger group and colleagues uncovered a basic three-neuron brainstem circuit underlying the reflexive blink [24, 28]. When the reflex must be modified or adapted, an additional cerebellar component of the circuit activates in the PIP [23, 28]. These results have been further supported by work done in alert behaving cats [50, 51]. In the latter model system, the PIP was further implicated in the control and enhancement of the conditioned blink. Conditioned blink-related activity in the PIP arose during the course of conditioning [50-56], and direct stimulation of the PIP resulted in eyelid responses [50]. However, blink-related responses in the PIP arose after the onset of the conditioned response [51], suggesting PIP neurons contribute to the control and enhancement of the conditioned blink. This is in contrast to the more direct role AIP neurons are thought to play in the initiation of the conditioned blink (see above). The study presented in this manuscript provides evidence of an anatomical connection between the anterior cerebellum and blink-related areas of the PIP. This corticonuclear projection further suggests that the anterior cerebellar cortex may be involved in the adaptive modulation of reflexes and the modulation and control of conditioned responses.

The final tract uncovered in the course of these studies runs from the posterior vermal/paravermal areas of the CbCtx to the FN. This tract involves some of the least-understood areas of the cerebellum, which are generally thought to be involved in motor coordination [57-60]. The fastigial nucleus is known to modulate movements via the vestibular nucleus and downstream motor nuclei [13, 22]. Results presented in this body of work show that a vestibulorubral connection exists in the mouse, providing a basic path of anatomical connectivity that may allow the posterior vermis and paravermis to coordinate movement via a fastigio-vestibulo-rubral circuit.

CONCLUSION

The distinct and parallel circuits revealed by this project may have implications in general cerebellar function. The "fractured somatotopy" of the cerebellar cortex is well established – that is, a single anatomical feature is represented in several locations on the cortex [58-60]. The results presented in these experiments suggest this fracturing of the body map is functionally organized. Thus, a given portion of the body may be represented in several locations in the cerebellum because each location serves a functionally distinct circuit. The cerebellar hemispheres and the dentate and anterior interpositus nuclei have already been closely tied to associative learning and classical conditioning. The anterior cerebellum and posterior interpositus are likely to be involved in reflex modulation. The posterior cerebellum and fastigial nuclei may, via projections through the vestibular and red nuclei, be involved in movement coordination.

The possibility of functional organization of the cerebellar corticonuclear circuits can be further explored by using two functionally similar but anatomically distinct learning models. For example, both eyeblink and forelimb movement tasks can be adapted into associative learning, reflex modulation, and coordination paradigms. Neurons associated with classically conditioned eyeblinks and forelimb movements may be expected to localize to distinct but nearby areas of the hemispheric cerebellar cortex and the dentate and anterior interpositus nuclei, while neurons associated with reflex eyeblink and paw withdrawal modulation might localize instead to the anterior cerebellar cortex and the posterior interpositus nucleus. To better understand the functional compartmentalization of the cerebellum, it would be worthwhile to pursue the experimental verification the anatomical organization of multiple cerebellar-modulated motor systems, in multiple cerebellar memory and modulation paradigms.

LIST OF ABBREVIATIONS

BDA – biotinylated dextran amine

CbCtx – cerebellar cortex, including subdivisions
Crus 1 – Crus 1 of the ansiform lobule of the cerebellar cortical hemispheres

Crus 2 – Crus 1 of the ansiform lobule of the cerebellar cortical hemispheres

DCN – deep cerebellar nuclei, including subdivisions

DN – dentate nucleus

FN – fastigial nucleus

GFP (EGFP) – green fluorescent protein

HRP – horseradish peroxidase

HVI – lobule simplex of the cerebellar cortical hemispheres

HVII – ansiform lobule of the cerebellar cortical hemispheres

IPN – interpositus nucleus (PIP, posterior interpositus and AIP, anterior interpositus)

PRV – pseudorabies virus, including PRV-152, the eGFP-expressing strain of PRV

RN – red nucleus

Sim – lobule simplex of the cerebellar cortical hemispheres

VN – vestibular nuclei

7N – facial nucleus

n^{th} Cb – the n^{th} lobule of the cerebellar vermis and paravermis (example: 2^{nd} Cb, the 2^{nd} lobule of the cerebellar vermis and paravermis)

CONFLICTS OF INTEREST

The author declares no conflicts of interest.

ACKNOWLEDGEMENTS

This work was generously supported by the NIH and the Packard Foundation. The author is grateful to Dr. Mark J. Schnitzer for his support throughout the course of this project, and to Dr. Paul S. Buckmaster, Dr. Liqun Luo, and Dr. Robert M. Sapolsky for their insightful comments and advice. Dr. Botond Roska and Dr. Fang-Ping Chen provided invaluable guidance during the initial phase of this project. The author also thanks Dr. Isabelle Billig, Dr. Carey Balaban, and Dr. Gabriella Ugolini for many helpful discussions; Dr. Timothy McCulley, Dr. Glenn Cockerham, and Dr. Jane Li for their technical expertise; and Dr. Lynn Enquist for generously providing all viruses used in these experiments.

REFERENCES

[1] Sun LW. Transsynaptic tracing of conditioned eyeblink circuits in the mouse cerebellum. *Neuroscience.* **2012;** 203: 122-34.

[2] Buisseret-Delmas C, Angaut P. The cerebellar nucleocortical projections in the rat. A retrograde labelling study using horseradish peroxidase combined to a lectin. *Neurosci Lett.* **1988;** 84: 255-60.

[3] Dietrichs E. The cerebellar corticonuclear and nucleocortical projections in the cat as studied with anterograde and retrograde transport of horseradish peroxidase. III. The anterior lobe. *Anat Embryol (Berl).* **1981;** 162: 223-47.

[4] Dietrichs E. The cerebellar corticonuclear and nucleocortical projections in the cat as studied with anterograde and retrograde transport of horseradish peroxidase. IV. The paraflocculus. *Exp Brain Res.* **1981;** 44: 235-42.

[5] Dietrichs E. The cerebellar corticonuclear and nucleocortical projections in the cat as studied with anterograde and retrograde transport of horseradish peroxidase. V. The posterior lobe vermis and the flocculonodular lobe. *Anat Embryol (Berl).* **1983;** 167: 449-62.

[6] Dietrichs E, Walberg F. The cerebellar corticonuclear and nucleocortical projection in the cat as studied with anterograde and retrograde transport of horseradish peroxidase. I. The paramedian lobule. *Anat Embryol (Berl).* **1979;** 158: 13-39.

[7] Dietrichs E, Walberg F. The cerebellar corticonuclear and nucleocortical projections in the cat as studied with anterograde and retrograde transport of horseradish peroxidase. II. Lobulus simplex, crus I and II. *Anat Embryol (Berl).* **1980;** 161: 83-103.

[8] Yeo CH, Hardiman MJ, Glickstein M. Classical conditioning of the nictitating membrane response of the rabbit. II. Lesions of the cerebellar cortex. *Exp Brain Res.* **1985;** 60: 99-113.

[9] Yeo CH, Hardiman MJ, Glickstein M. Classical conditioning of the nictitating membrane response of the rabbit. I. Lesions of the cerebellar nuclei. *Exp Brain Res.* **1985;** 60: 87-98.

[10] Sugihara I. Compartmentalization of the deep cerebellar nuclei based on afferent projections and aldolase C expression. *Cerebellum.* **2011;** 10: 449-63.

[11] Sugihara I, Fujita H, Na J, Quy PN, Li BY, Ikeda D. Projection of reconstructed single Purkinje cell axons in relation to the cortical and nuclear aldolase C compartments of the rat cerebellum. *J Comp Neurol.* **2009;** 512: 282-304.

[12] Sugihara I, Shinoda Y. Molecular, topographic, and functional organization of the cerebellar nuclei: analysis by three-dimensional mapping of the olivonuclear projection and aldolase C labelling. *J Neurosci.* **2007;** 27: 9696-710.

[13] Diagne M, Delfini C, Angaut P, Buisseret P, Buisseret-Delmas C. Fastigiovestibular projections in the rat: retrograde tracing coupled with [gamma]amino-butyric acid and glutamate immunohistochemistry. *Neurosci Lett.* **2001;** 308: 49-53.

[14] Matesz C, Bácskai T, Nagy E, Halasi G, Kulik A. Efferent connections of the vestibular nuclei in the rat: a neuromorphological study using PHA-L. *Brain Res Bull.* **2002;** 57: 313-5.

[15] Aston-Jones G, Card JP. Use of pseudorabies virus to delineate multisynaptic circuits in brain: opportunities and limitations. *J Neurosci Methods.* **2000;** 103: 51-61.

[16] Banfield BW, Kaufman JD, Randall JA, Pickard GE. Development of pseudorabies virus strains expressing red fluorescent proteins: new tools for multisynaptic labelling applications. *J Virol.* **2003;** 77: 10106-12.

[17] Card JP, Enquist LW. Transneuronal circuit analysis with pseudorabies viruses. *Curr Protoc Neurosci.* **2001;** Chapter 1: Unit1.5.

[18] Enquist LW, Card JP. Recent advances in the use of neurotropic viruses for circuit analysis. *Curr Opin Neurobiol.* **2003;** 13: 603-6.

[19] Loewy AD. Pseudorabies Virus: A Transneuronal Tracer for Neuroanatomical Studies, in *Viral Vectors*, Michael G. Kaplitt, Arthur D. Loewy, Editors. **1995;** Academic Press: San Diego. 349-66.

[20] Nagayama S, Zeng S, Xiong W, Fletcher ML, Masurkar AV, Davis DJ, Pieribone VA, Chen WR. In vivo simultaneous tracing and Ca(2+) imaging of local neuronal circuits. *Neuron.* **2007;** 53: 789-803.

[21] Smith BN, Banfield BW, Smeraski CA, Wilcox CL, Dudek FE, Enquist LW, Pickard GE. Pseudorabies virus expressing enhanced green fluorescent protein: A tool for in vitro electrophysiological analysis of transsynaptically labelled neurons in identified central nervous system circuits. *Proc Natl Acad Sci U S A.* **2000;** 97: 9264-9.

[22] Boyden ES, Katoh A, Raymond JL. Cerebellum-dependent learning: the role of multiple plasticity mechanisms. *Annu Rev Neurosci.* **2004;** 27: 581-609.

[23] Chen FP, Evinger C. Cerebellar modulation of trigeminal reflex blinks: interpositus neurons. *J Neurosci.* **2006;** 26: 10569-76.

[24] Evinger C, Manning KA, Sibony PA. Eyelid movements. Mechanisms and normal data. *Invest Ophthalmol Vis Sci.* **1991;** 32: 387-400.

[25] Evinger C, Shaw MD, Peck CK, Manning KA, Baker R. Blinking and associated eye movements in humans, guinea pigs, and rabbits. *J Neurophysiol.* **1984;** 52: 323-39.

[26] Faulkner B, Brown TH, Evinger C. Identification and characterization of rat orbicularis oculi motoneurons using confocal laser scanning microscopy. *Exp Brain Res.* **1997;** 116: 10-9.

[27] Gong S, Zhou Q, LeDoux MS. Blink-related sensorimotor anatomy in the rat. *Anat Embryol (Berl).* **2003;** 207: 193-208.

[28] Henriquez VM, Evinger C. The three-neuron corneal reflex circuit and modulation of second-order corneal responsive neurons. *Exp Brain Res.* **2007;** 179: 691-702.

[29] Holstege G, van Ham JJ, Tan J. Afferent projections to the orbicularis oculi motoneuronal cell group. An autoradiographical tracing study in the cat. *Brain Res.* **1986;** 374: 306-20.

[30] Martin MR, Lodge D. Morphology of the facial nucleus of the rat. *Brain Res.* **1977;** 123: 1-12.

[31] Morcuende S, Delgado-Garcia JM, Ugolini G. Neuronal premotor networks involved in eyelid responses: retrograde transneuronal tracing with rabies virus from the orbicularis oculi muscle in the rat. *J Neurosci.* **2002;** 22: 8808-18.

[32] Shaw MD, Baker R. Direct projections from vestibular nuclei to facial nucleus in cats. *J Neurophysiol.* **1983;** 50: 1265-80.

[33] Shaw MD, Baker R. Morphology of motoneurons in a mixed motor pool of the cat facial nucleus that innervate orbicularis oculis and quadratus labii superioris, stained intracellularly with horseradish peroxidase. *Neuroscience.* **1985;** 14: 627-43.

[34] Trigo JA, Gruart A, Delgado-García JM. Discharge profiles of abducens, accessory abducens, and orbicularis oculi motoneurons during reflex and conditioned blinks in alert cats. *J Neurophysiol.* **1999;** 81: 1666-84.

[35] Buisseret-Delmas C, Angaut P. Anatomical mapping of the cerebellar nucleocortical projections in the rat: a retrograde labelling study. *J Comp Neurol.* **1989;** 288: 297-310.

[36] Sugihara I, Shinoda Y. Shinoda, Molecular, topographic, and functional organization of the cerebellar cortex: a study with combined aldolase C and olivocerebellar labelling. *J Neurosci.* **2004;** 24: 8771-85.

[37] Lavond DG, Hembree TL, Thompson RF. Effect of kainic acid lesions of the cerebellar interpositus nucleus on eyelid conditioning in the rabbit. *Brain Res.* **1985;** 326: 179-82.

[38] Racine RJ, Wilson DA, Gingell R, Sunderland D. Long-term potentiation in the interpositus and vestibular nuclei in the rat. *Exp Brain Res.* **1986;** 63: 158-62.

[39] Berthier NE, Moore JW. Cerebellar Purkinje cell activity related to the classically conditioned nictitating membrane response. *Exp Brain Res.* **1986;** 63: 341-50.

[40] Lavond DG, Steinmetz JE. Acquisition of classical conditioning without cerebellar cortex. *Behav Brain Res.* **1989;** 33: 113-64.

[41] Woodruff-Pak DS, Lavond DG, Logan CG, Steinmetz JE, Thompson RF. Cerebellar cortical lesions and reacquisition in classical conditioning of the nictitating membrane response in rabbits. *Brain Res.* **1993;** 608: 67-77.

[42] Gould TJ, Steinmetz JE. Multiple-unit activity from rabbit cerebellar cortex and interpositus nucleus during classical discrimination/reversal eyelid conditioning. *Brain Res.* **1994;** 652: 98-106.

[43] Hesslow G, Ivarsson M. Suppression of cerebellar Purkinje cells during conditioned responses in ferrets. *Neuroreport.* **1994;** 5: 649-52.

[44] Attwell PJ, Rahman S, Ivarsson M, Yeo CH. Cerebellar cortical AMPA-kainate receptor blockade prevents performance of classically conditioned nictitating membrane responses. *J Neurosci.* **1999;** 19: RC45.

[45] Perrett SP, Ruiz BP, Mauk MD. Cerebellar cortex lesions disrupt learning-dependent timing of conditioned eyelid responses. *J Neurosci.* **1993;** 13: 1708-18.

[46] Mauk MD, Donegan NH. A model of Pavlovian eyelid conditioning based on the synaptic organization of the cerebellum. *Learn Mem.* **1997;** 4: 130-58.

[47] Garcia KS, Steele PM, Mauk MD. Cerebellar cortex lesions prevent acquisition of conditioned eyelid responses. *J Neurosci.* **1999;** 19: 10940-7.

[48] Medina JF, Garcia KS, Nores WL, Taylor NM, Mauk MD. Timing mechanisms in the cerebellum: testing predictions of a large-scale computer simulation. *J Neurosci.* **2000;** 20: 5516-25.

[49] Kalmbach BE, Davis T, Ohyama T, Riusech F, Nores WL, Mauk MD. Cerebellar cortex contributions to the expression and timing of conditioned eyelid responses. *J Neurophysiol.* **2010;** 103: 2039-49.

[50] Gruart A, Guillazo-Blanch G, Fernández-Mas R, Jiménez-Díaz L, Delgado-García JM. Cerebellar posterior interpositus nucleus as an enhancer of classically conditioned eyelid responses in alert cats. *J Neurophysiol.* **2000;** 84: 2680-90.

[51] Jiménez-Díaz L, Navarro-López Jde D, Gruart A, Delgado-García JM. Role of cerebellar interpositus nucleus in the genesis and control of reflex and

conditioned eyelid responses. *J Neurosci.* **2004;** 24: 9138-45.
[52] Berthier NE, Moore JW. Activity of deep cerebellar nuclear cells during classical conditioning of nictitating membrane extension in rabbits. *Exp Brain Res.* **1990;** 83: 44-54.
[53] Steinmetz JE, Lavond DG, Ivkovich D, Logan CG, Thompson RF. Disruption of classical eyelid conditioning after cerebellar lesions: damage to a memory trace system or a simple performance deficit? *J Neurosci.* **1992;** 12: 4403-26.
[54] Ivkovich D, Lockard JM, Thompson RF. Interpositus lesion abolition of the eyeblink conditioned response is not due to effects on performance. *Behav Neurosci.* **1993;** 107: 530-2.
[55] Krupa DJ, Thompson RF. Reversible inactivation of the cerebellar interpositus nucleus completely prevents acquisition of the classically conditioned eye-blink response. *Learn Mem.* **1997;** 3: 545-56.
[56] McCormick DA, Thompson RF. Cerebellum: essential involvement in the classically conditioned eyelid response. *Science.* **1984;** 223: 296-9.
[57] Voogd J, Glickstein M. The anatomy of the cerebellum. *Trends Neurosci.* **1998;** 21: 370-5.
[58] Kandel E, Schwartz JH, Jessell T. Principles of Neural Science. **2000**: McGraw-Hill Medical.
[59] Nieuwenhuys R, Donkelaar HJ, Nicholson C. The Central Nervous System of Vertebrates. **1998**: Springer-Verlag.
[60] Lowrie M, Conn PM. ed., *Neuroscience in medicine*. 2nd edition. New Jersey: The Humana Press, **2003**.